# Computing the Atmospheric Absorption for the DMSP Operational Linescan System Infrared Channel

THOMAS J. GREENWALD

*Cooperative Institute for Research in the Atmosphere, Colorado State University, Fort Collins, Colorado*

CHARLES J. DRUMMOND

*Department of Atmospheric Science, Colorado State University, Fort Collins, Colorado*

(Manuscript received 7 August 1998, in final form 27 January 1999)

ABSTRACT

An accurate and rapid means is presented for computing the atmospheric absorption for the infrared channel (10.2–12.7 $\mu$m) on the Defense Meteorological Satellite Program operational linescan system (OLS) for use in remote sensing studies of surface and cloud properties. The method is a new approach to correlated *k*-distribution theory that keeps track of spectral information at the cumulative probability (*g*) level and more effectively addresses overlapping absorption through a recursive procedure. It also incorporates details of the instrument's response function. Comparisons with line-by-line (LBL) results demonstrate that calculations using only 60 *g*-space intervals produce total atmospheric transmittance errors of 0.24% for a tropical atmosphere and 1.2% for a midlatitude winter atmosphere. In terms of upwelling equivalent blackbody (EBB) temperatures computed at the top of the atmosphere (TOA), the errors are less than 0.5 K over a wide range of atmospheric profiles and zenith angles when compared to LBL radiative transfer calculations. Errors are smallest ($<$0.1 K) for tropical environments. For downwelling EBB temperatures at the surface the errors become somewhat larger, especially for the winter atmosphere (maximum error of 1.66 K). Errors also generally increase slightly with increasing zenith angle. Reducing the number of *g*-space intervals to 17 can still provide reasonable results with a maximum error of 0.72 K for the TOA upwelling EBB temperature in a midlatitude winter atmosphere.

## 1. Introduction

The operational linescan system (OLS) on the Defense Meteorological Satellite Program (DMSP) satellites has been a highly reliable visible/infrared (IR) sensor for the Department of Defense (DOD) for over two decades. As the primary DMSP weather sensor, its purpose is to support worldwide DOD activities by providing global imagery to aid military weather forecasters and tactical military operations. While the OLS is intended for operational use, there has been an increasing interest in it for environmental monitoring and basic scientific research (e.g., Cahoon 1992; Goodman and Christian 1993; Fett 1993). As for the future of the OLS, plans (scheduled for 2002) are to include two near-IR channels (1.5–1.64 and 3.5–3.9 $\mu$m) and two split-window channels (10.3–11.3 and 11.5–12.5 $\mu$m) to replace the one IR channel (R. Carrell 1998, personal communication).

Besides identifying cloud systems and surface features and providing cloud-top temperature (Isaacs and Barnes 1987), the OLS IR channel has other potential scientific uses. For example, Cogan (1976) and Brandli et al. (1977) looked at the possibility of using this channel to estimate sea surface temperature (SST). May (1993) extended and improved upon this idea using data from the Special Sensor Microwave/Imager (SSM/I) to correct for water vapor attenuation. Another possible application is to estimate land surface skin temperature to help in deriving surface microwave emissivity in clear regions (e.g., Jones and Vonder Haar 1997).

The main goal of this study is to predict efficiently and accurately the atmospheric absorption for the OLS IR channel for use in quantitative research applications. This is achieved using a new approach to the correlated *k* (absorption coefficient)-distribution method developed by Drummond and Stephens (1998), which was applied to the Moderate Resolution Imaging Spectroradiometer Airborne Simulator instrument. This approach is different because it retains spectral information, which allows for overlapping absorption by multiple gases to be dealt with more efficiently and accounts for the full details of the instrument's spectral response. Because of its moderately broad bandwidth (10.2–12.7

*Corresponding author address:* Dr. Thomas J. Greenwald, CIRA, Colorado State University, Fort Collins, CO 80523.
E-mail: greenwald@cira.colostate.edu

$\mu$m), characterizing the gaseous absorption for the OLS IR channel requires more careful consideration than typical narrowband satellite sensors [e.g., the Advanced Very High Resolution Radiometer (AVHRR)]. To our knowledge, a detailed investigation of this kind has yet to be carried out for the OLS IR channel.

Another objective is to raise a greater awareness in the research community of this largely underutilized instrument. In this light, a description of the OLS is provided in the following section, including simple calibration tests for the IR measurements to support their use for quantitative remote sensing. A brief discussion of the line-by-line (LBL) gaseous absorption calculations is given in section 3, which are high spectral resolution data used in creating the *k* distributions. A synopsis of the correlated *k*-distribution method is given in section 4 along with a description of the new approach. In section 5, the validity of the new method is tested by comparing radiance calculations, using the correlated *k*-distribution-derived atmospheric absorption, to LBL radiance calculations under a large range of clear-sky atmospheric conditions and varying satellite-viewing geometry. This is followed by a summary discussion in the final section.

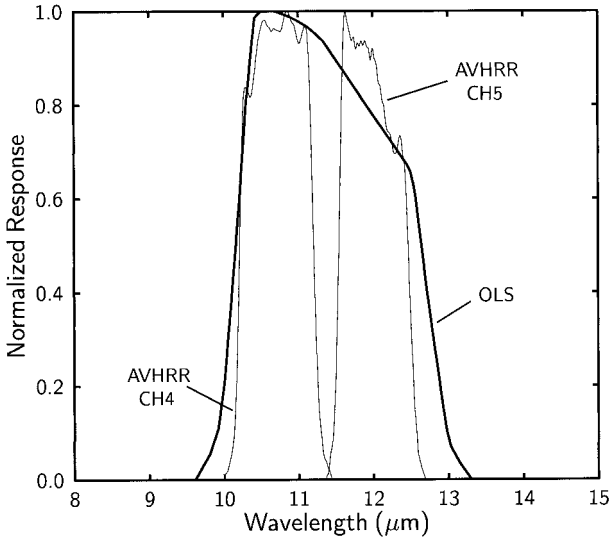


FIG. 1. Normalized spectral response curve for the operational linescan system (OLS) infrared channel. Also shown are the response curves for the split-window channels (4 and 5) on the *NOAA-9* AVHRR.

## 2. The operational linescan system (OLS)

### *a. Instrument description*

The OLS is a dual-channel radiometric system for collecting radiance measurements at visible and infrared wavelengths at all times of the day. The system essentially consists of a scanning telescope, an arrangement of optics, a mercury–cadmium–telluride detector for sensing IR radiation and two separate detectors that compose the visible channel: a silicon detector and a photomultiplier tube (PMT). The half-power response bandwidths of the two channels are 0.58–0.96 $\mu$m (silicon detector) and 10.16–12.65 $\mu$m (IR). Onboard calibration of the thermal channel is performed using cold and hot calibration sources of known temperature, while the visible channel uses a dark calibration source. The visible channel allows for a very large dynamic range of illumination (approximately $10^7$). The gain is continuously adjusted across an image to compensate for the wide differences in solar illumination that occur near the terminator. This is achieved automatically using a switchable gain amplifier controlled by a digital processor in addition to information regarding the scan angle and solar geometry. One minor drawback of the IR channel is that its dynamic range (210–310 K) is somewhat limited for extremely cold cloud temperatures, where the channel can become saturated (Isaacs and Barnes 1987). The PMT provides visible imagery (0.5–0.85 $\mu$m) at night, which makes possible the optical detection of man-made and natural fires (Cahoon 1992) and lightning events (Goodman and Christian 1993), among other phenomena. The primary mirror of the OLS moves in a sinusoidal fashion. This motion, along with a variable instantaneous field of view, helps to keep a nearly constant effective footprint dimension of each element throughout the scan (Spangler 1974; Isaacs and Barnes 1987). The swath width of the OLS on the ground is roughly 2960 km.

The IR channel has a rather broad bandwidth in comparison to other weather sensors. Prior to June 1979, however, the spectral bandwidth was even wider, nearly twice that of the current IR channel (Spangler 1974; Isaacs and Barnes 1987). Figure 1 depicts the normalized spectral response function for the current IR channel. For comparison, the response functions for the split-window channels of the *NOAA-9* AVHRR are also shown. The OLS response curve is a function of the bandpass filter, the detector, the antireflection coating on the refractive lens, the beamsplitter, the lens elements, folding mirrors, and the telescope mirrors. Over this spectral range the chief gaseous absorbers are water vapor, $CO_2$, and $0_3$.

Data collected by the detectors (except at nighttime low light levels) have 6-bit precision with a spatial resolution of about 0.6 km, which is called ''fine'' resolution data. The noise equivalent temperature differential (NE$\Delta$T) of the IR channel at this resolution is about 1.9 K (May 1993). To store a full orbit's worth of data on the data recorders, these data are averaged aboard the satellite by electronically filtering along the scan and digitally averaging in the along-track direction (Spangler 1974). These ''smooth'' resolution data are kept at 8-bit precision and have a spatial resolution of 2.8 km. For these data the NE$\Delta$T significantly reduces to roughly 0.47 K (May 1993). The smooth data are

TABLE 1. Near-time-coincident, collocated *F10* and *F12* OLS IR equivalent blackbody (EBB) temperatures ($T_{ebb}$) and statistics for clear-sky ocean scenes in two different geographical regions. Here *N* is number of data points, and rms is root mean square.

| *F10* mean $T_{ebb}$ (K) | *F12* mean $T_{ebb}$ (K) | Bias (K) | rms (K) | *N* |
|---|---|---|---|---|
| 273.19 | 273.16 | 0.03 | 0.51 | 1665 |
| 291.71 | 291.89 | −0.18 | 0.61 | 4497 |

particularly useful for remote sensing studies because of their far lower noise levels.

### b. IR channel calibration tests

Calibration of the OLS IR channel measurements is often viewed as not measuring up to the necessary high standards required for quantitative remote sensing studies. The objective here is to demonstrate the integrity of the IR channel calibration using two simple tests. First, an intercalibration was performed for near-coincident overlapping smooth IR imagery from the DMSP *F10* and *F12* satellites. Data were selected at 1023 and 0951 UTC 6 January 1995, respectively, in the North Pacific. Only clear-sky ocean pixels were selected because they provide highly homogeneous scenes. Data were collocated at the pixel level.

The results of the comparison are given in Table 1 for two regions of warm and cold temperatures. The root-mean-square (rms) differences between the sensors are comparable to the noise level of the measurements. Also, the biases are notably small. For the warm temperature case where the atmospheric attenuation is the greatest, the slight bias may be caused in part by differences in the viewing angles between the sensors since there was about a 140-km cross-track alignment difference between the images. Granted, this is only a relative comparison, but it does demonstrate that, at least for this range of temperatures and for these two sensors, the intercalibration is very good.

A second test to provide a more absolute assessment of the calibration is to obtain an independent estimate of the surface emission and then compare it to the OLS measurements for the cold temperature case (located near the Kamchatka Peninsula). Under these conditions the atmospheric attenuation is negligible and the sensor is seeing the surface nearly unimpeded (the SSM/I indicated column water vapor values of 3–4 kg $m^{-2}$). It is assumed the emissivity of the ocean surface at 11 $\mu$m is 0.99 (Buettner and Kern 1965) and the SST approximates the ocean skin temperature. Using a mean SST in this region of 275.2 $\pm$ 0.3 K from the weekly 1° gridded SST analyses of Reynolds, we obtain an equivalent blackbody (EBB) temperature estimate of 274.6 $\pm$ 0.3 K for the surface emission. Accounting for atmospheric attenuation in the OLS measurements ($\approx$1.5 K), this estimate is in excellent agreement with the OLS measurements (see Table 1). Clearly, these results give added confidence in the absolute calibration of the IR channel on these sensors, which, based on these limited results, is certainly within about 1 K for EBB temperatures near 273 K.

## 3. Line-by-line molecular absorption spectra

The highest resolution data available for describing the spectral absorption characteristics of active molecules in the atmosphere are referred to as line-by-line (LBL) spectra. These data are used in deriving the *k* distributions, which are discussed in the next section. The LBL absorption spectra are computed based on information concerning the line strength, ground state energy, and broadening characteristics for all relevant gases. The LBL data used here were obtained from the molecular transition line database of HITRAN (Rothman et al. 1992). A closed form of the Voigt profile from Formichev and Shved (1995) was applied for Doppler and Lorentz broadening. In addition to resonance line absorption, $H_20$ continuum absorption also occurs throughout the OLS IR bandwidth. This continuum was accounted for in Drummond and Stephens (1998) using the parameterization of Roberts et al. (1976). However, this study uses version 2.2 of the Clough parameterization (e.g., Clough et al. 1989), which is generally considered to be a more accurate representation of the $H_20$ continuum in the 8–12-$\mu$m window.

The LBL absorption coefficient spectra are computed for each gas at 26 reference pressure levels (0.1–1000 mb) and three reference temperatures (210, 250, 290 K) with an approximate resolution of 0.004 $cm^{-1}$. These calculations were one of the most computationally intensive parts of the study. To significantly ease the computational burden, two distinct types of optimization were utilized. Drummond and Stephens (1998) discuss these optimization schemes and provide other details regarding the LBL *k*-spectra calculations.

## 4. Correlated *k*-distribution method

The approach chosen for modeling the effects of gaseous absorption on OLS IR measurements is an extension of the well-known *k*-distribution method. Because the magnitude of the absorption coefficient (*k*) for a gas is likely to be repeated more than once over a given spectral band, the *k*-distribution method exploits this fact by transforming the spectral absorption coefficients into cumulative probability (*g*) space. This ''reordered'' distribution has the equivalent transmission properties as the original distribution in spectral space yet it is much smoother and is thus more desirable for absorption calculations. This idea was originally developed by Ambartzumian (1936) and first applied to terrestrial atmospheres by Lacis and Hansen (1974).

An appreciation of the power of *k*-distribution theory can be gained by illustrating the LBL method for com-

puting the mean atmospheric transmission across a spectral region. For a single gas over a homogeneous path, the band-average transmission across a wavenumber interval $[\nu_1, \nu_2]$ is

$$T(u) = \frac{1}{\nu_2 - \nu_1} \int_{\nu_1}^{\nu_2} \exp(-k_\nu u)\, d\nu, \qquad (1)$$

where $u$ is the absorber amount (absorber density integrated over the pathlength) and $k_\nu$ is the absorption coefficient as a function of wavenumber. Using the LBL approach, numerical evaluation of (1) usually involves several thousand or more calculations over the bandwidth of a typical narrowband instrument. The essence of the $k$-distribution method is expressing the transmission in terms of integration over $k$ space as

$$T(u) = \frac{1}{\nu_2 - \nu_1} \int_0^\infty f(k) \exp(-ku)\, dk, \qquad (2)$$

where $f(k)$ is a probability distribution function for the absorption coefficients across the wavenumber interval. This expression also defines $f(k)$ as having $T(u)$ as its Laplace transform. In practice, $f(k)$ is derived in discrete form by grouping the LBL absorption coefficients into bins of width $\Delta k$ normalized to unity over the wavenumber interval.

Unfortunately, many calculations are still required to faithfully evaluate Eq. (2). As a solution to this problem, $f(k)$ is converted to a *cumulative* probability (or distribution) function (which ranges from 0 to 1) through

$$g(k) = \int_0^k f(k')\, dk'.$$

The so-called $k$ distribution simply follows as

$$k(g) = g^{-1}(k).$$

In $g$ space the band-averaged total transmission becomes

$$T(u) = \int_0^1 \exp[-k(g)u]\, dg \approx \sum_{i=1}^{N} \exp[-k(g_i)u]\Delta g_i. \qquad (3)$$

The key advantage of this transformation becomes clear from (3). Since $k(g)$ is a highly smooth function, the integral can be approximated numerically to a high degree of accuracy using only a small number of discrete $g$ intervals (i.e., $\Delta g$'s). Other major advantages of the $k$-distribution theory are that it is applicable to scattering problems and that it can be used for wide spectral regions that are not statistically homogeneous, unlike band model theory (Goody and Yung 1989).

The $k$-distribution method is strictly valid for homogeneous paths. The development of the *correlated* $k$-distribution (CKD) method was intended to extend the $k$-distribution method to include the effects of pressure and temperature changes along the path for its applicability in realistic atmospheres. The idea of the CKD method is that the $k$ distributions at all pressures and temperatures are correlated in $\nu$ space over an interval $[\nu_1, \nu_2]$ (Lacis and Oinas 1991). For the interested reader, Fu and Liou (1992) and Lacis and Oinas (1991) provide thorough and lucid discussions of the physical basis for the CKD method and its accuracy in the context of computing infrared and solar radiation heating rates.

Subsequent development focused on extending the CKD method to include the effects of overlapping absorption by multiple gas species in nonhomogeneous atmospheres (e.g., Lacis and Oinas 1991). The most common strategy for dealing with overlapping absorption is to apply the multiplication transmissivity property (Goody and Yung 1989), whereby the total spectral–mean transmittance for any number of different gases is simply given as the multiplication of the individual transmittances for these gases (assuming the gases do not interact). Given $n$ number of gases the spectral–mean total transmittance is expressed in terms of $g$ as

$$T_{\bar{\tau}}(1, 2, \ldots, n) = \int_0^1 \cdots \int_0^1 \exp\{-[k(g_1) + \cdots + k(g_n)]u\}\, dg_1 dg_2, \ldots, dg_n. \qquad (4)$$

While this approach can produce very good results, it becomes immediately apparent that the nested integrals in (4) involve numerous calculations since the number of calculations goes like $N_1 \times N_2 \times \cdots \times N_n$, where $N_n$ is the number of discrete $g$ intervals for gas $n$. Furthermore, evaluation of (4) produces combinations of $k$ that are unphysical, thus requiring unnecessary additional calculations that make the method rather inefficient.

To overcome the complications and inefficiencies in previous attempts to treat overlapping absorption in the CKD method, an alternative and novel approach is used here that permits a recursive treatment of overlapping absorption, thus minimizing the occurrence of nonphysical overlap. This idea is actually part of a broader philosophy that seeks to keep track of spectral information at the $g$-space level—information that is often lost in conventional CKD methods—while applying an error minimization technique that ensures a computationally efficient and accurate method. This approach has been found to be generally robust and easily allows for the characterization of source functions and the incorporation of instrument response (or filter) functions at the $g$-space level.

When multiple gases are present within a spectral band, the first step in this process is to sort the absorbers into increasing column transmission order, where the strongest absorber is considered first (for the case of the OLS it was $CO_2$). Reference $k$ distributions [i.e., $k(g)$'s] were constructed from the LBL $k$ spectra for $CO_2$ at the 26 reference pressures and three reference temperatures.

Creation of these distributions consisted of 1000 bins ($\Delta k$'s) per decade of $k$ strength (the $\log_{10}$ of $k$ is used) to adequately resolve rapidly changing features in the probability distribution functions [$f(k)$'s], following the approach of Lacis and Oinas (1991).

The next step is to apply an error minimization technique to determine a set of $\Delta g$ intervals for the first absorber (i.e., $\Delta g_{\mathrm{CO}_2}$) that meet the following error criteria for absolute transmission ($\overline{\varepsilon}_a$) and relative absorption ($\overline{\varepsilon}_r$) for each $\Delta g_{\mathrm{CO}_2}$ interval $j$ as

$$\overline{\varepsilon}_a(j) > \frac{1}{N_p N_u} \sum_{i=1}^{N_p} \sum_{m=1}^{N_u} |T_{k(g)}(j, i, m) - T_{k_{\mathrm{eff}}}(j, i, m)|$$

$$\overline{\varepsilon}_r(j) > \frac{1}{N_p N_u} \frac{\sum_{i=1}^{N_p} \sum_{m=1}^{N_u} |T_{k_{\mathrm{eff}}}(j, i, m) - T_{k(g)}(j, i, m)|}{\sum_{i=1}^{N_p} \sum_{m=1}^{N_u} |1 - T_{k(g)}(j, i, m)|},$$

where $N_p$ is the number of reference pressure levels (i.e., 26), $N_u$ is the number of values of $u$ used per pressure level (i.e., 20) to represent a realistic range of $u$ [as determined from McClatchey et al. (1972) and profiles from the *U.S. Standard Atmosphere, 1976*], and $T_{k(g)}(j, i, m)$ is the $j$th interval-averaged transmission for each $u$ and reference pressure, given as

$$T_{k(g)}(j, i, m) = \frac{\sum_{l=b_1}^{b_2} \exp[-k(i, g_l)u_m]\Delta g_l}{\sum_{l=b_1}^{b_2} \Delta g_l},$$

and $T_{k_{\mathrm{eff}}}(j, i, m) = \exp[-k_{\mathrm{eff}}(j, i)u_m]$, where the desired quantity (i.e., the weighted average of $k$ within a $\Delta g_{\mathrm{CO}_2}$ interval) is

$$k_{\mathrm{eff}}(j, i) = \frac{\sum_{l=b_1}^{b_2} k(i, g_l)\Delta g(l)}{\sum_{l=b_1}^{b_2} \Delta g(l)}$$

and $b_1$ and $b_2$ are the range of the bin indices for the $\Delta k$ bins. Two different error criteria are used so as to eliminate cases in which very small absolute transmission errors produce large relative absorption errors. A two-level error minimization algorithm involving an iterative procedure is utilized whereby $k(g)$ is discretized into smaller and smaller $\Delta g_{\mathrm{CO}_2}$ intervals until the error criteria are met. Details concerning the algorithm can be found in Drummond and Stephens (1998).

Once the errors have been successfully minimized for the first gas, new $k$ distributions are then constructed from the $k$ spectra for the next strongest gas (which in this case is $H_2O$) using the wavenumber intervals that occur within the first $\Delta g_{\mathrm{CO}_2}$ interval. Recall that in the $k$-distribution method the wavenumber (or spectral) information has been jumbled so that wavenumbers occurring anywhere within the instrument spectral band can appear in a given $\Delta g$ interval. The new approach here is to apply, in essence, a bookkeeping method that keeps track of the wavenumber intervals occurring within each $\Delta g$ interval, information that can be recalled when required [see Drummond and Stephens (1998) for details].

The goal in dealing with the second absorber is to find instead new $\Delta g$ intervals (i.e., $\Delta g_{\mathrm{H_2O}}$) for the first $\Delta g_{\mathrm{CO}_2}$ interval through the error minimization procedure. In this way, effort is not duplicated as is inherent when using the multiplication transmissivity property. The process outlined previously for the first gas is then repeated for each $\Delta g$ interval until all $\Delta g$ subintervals relevant to the second absorber are determined.

After completing this process for the last absorber (i.e., $O_3$), a hierarchy of $\Delta g$ intervals for each gas is formed. The final set of $\Delta g$ intervals defined for the spectral band of interest is derived as follows for each $j$th interval as

$$\Delta g(j) = \prod_{l=1}^{N} \Delta g(l),$$

where $\Delta g(l)$ is the subinterval for gas, $l$; $N$ is the total number of gases (here, $N = 3$); and the condition $\Sigma_j \Delta g_j = 1$ holds. We should note that the description of the overall method provided here is simply an overview. There are also many important details regarding specific programming and computational aspects that are provided by Drummond and Stephens (1998).

At this point, the appropriate $\Delta g$ intervals and the interval-averaged effective absorption coefficients ($k_{\mathrm{eff}}$'s) for the reference pressures and temperatures for each gas are known. To use the $k_{\mathrm{eff}}$'s for any arbitrary temperature ($T$), Drummond and Stephens (1998) applied a quadratic fit for $k_{\mathrm{eff}}$ as a function of $T - 250$ K, or, upon failure of this fit, a linear interpolation was used. In this study neither of these interpolation schemes was found to be adequate for temperatures between 210 and 250 K for the $CO_2$ absorption bands. Thus a linear fit for the $\log_{10}$ of $k_{\mathrm{eff}}$ was used instead, which was found to greatly improve the results. A linear interpolation of the $\log_{10}$ of $k_{\mathrm{eff}}$ was also used to determine $k_{\mathrm{eff}}$'s at any arbitrary pressure. Finally, the optical depth $\tau$ for a layer of gas, $i$, is determined from

$$\tau_i = \exp[-\overline{k}_{\mathrm{eff}}(i)u],$$

where $\overline{k}_{\mathrm{eff}}(i)$ is the interpolated absorption coefficient for the layer.

Because the wavenumber information within each $\Delta g$ interval is tracked, the mean source functions (in our case the Planck blackbody emission) and the mean instrument response can be computed for each $\Delta g$ interval. This allows for easy incorporation of the full instrument response function into radiative transfer calculations, which is an important advantage over conventional

TABLE 2. Band-averaged (response function weighted) total atmospheric transmittances for the operational linescan system using line-by-line (LBL) and 60 g-space-correlated *k*-distribution (CKD) calculations for different clear-sky atmospheres. TPW is total precipitable water.

| Profiles | TPW (kg m$^{-2}$) | LBL | CKD | Error (%) |
|---|---|---|---|---|
| Midlatitude winter | 8.7 | 0.9072 | 0.8960 | −1.2 |
| Midlatitude summer | 27 | 0.6227 | 0.6204 | −0.37 |
| Tropical | 42 | 0.4604 | 0.4615 | 0.24 |

CKD methods that have been applied to instruments (e.g., Kratz 1995).

Given this information and a radiative transfer model, the band-averaged radiance can be derived as follows:

$$I_{\overline{\nu}} = \frac{\sum_{i=1}^{N} I_i \Delta g_i \overline{\Phi}_i}{\sum_{i=1}^{N} \Delta g_i \overline{\Phi}_i},$$

where $I_i$ is the computed radiance for an interval $\Delta g_i$, $\overline{\Phi}_i$ is the mean response of the instrument over $\Delta g_i$, and $N$ is the total number of $\Delta g$ intervals. For the OLS IR channel, $N = 60$. Conversion of $I_{\overline{\nu}}$ to EBB temperature applies the Planck function and assumes a weighted-band average wavelength of 11.358 $\mu$m. The *k*-distribution parameter database for the OLS IR channel and copies of the source code that read the data (written in C and FORTRAN 90) are available from the authors.

## 5. Results

Several atmospheric profiles were used to assess the performance of the derived *k*-distribution parameters. Three representative profiles from McClatchey et al. (1972) were selected: the tropical (TR), midlatitude summer (MLS), and midlatitude winter (MLW) profiles (surface temperatures are 300.0, 294.0, and 272.2 K, respectively). A surface emissivity of 1.0 was assumed. Top-of-atmosphere (TOA) radiances were calculated using an eight-stream plane-parallel doubling/adding radiative transfer (RT) model. Over the bandwidth of the OLS IR channel the number of LBL RT calculations exceeded 70 000. These LBL calculations were also modified by the OLS response function.

We emphasize that in determining the errors between the LBL and CKD RT calculations it is naturally assumed that the humidity and temperature profiles and surface temperature and emissivity are known exactly. Our goal here is to isolate the errors due entirely to the CKD method. In retrievals of surface skin temperature, for example, uncertainties in the atmospheric profiles and surface IR emissivity will introduce further errors. This study does not address these other potentially important error sources.

The CKD method (60 $\Delta g$ intervals) reproduces the band-averaged total transmittances best for the TR and MLS profiles, as compared to the LBL results (Table 2). There is a tendency, however, for the CKD method to underestimate the transmittances for profiles with less water vapor, while slightly overestimating the transmittance for the tropical profile. A more interesting behavior of these results is that the transmittance error *decreases* with increasing total water vapor abundance. This is mainly a consequence of the CKD method's ability to better represent the $k(g)$ function for more strongly absorbing paths since this function is typically somewhat flatter than for the case of weaker absorption.

The CKD parameters perform very well in comparison to the LBL calculations for upwelling TOA radiances and EBB temperatures (Table 3). The lowest systematic errors occur for the TR and MLS atmospheres, where differences in TOA EBB temperatures of less

TABLE 3. Clear-sky top-of-atmosphere upwelling radiances and equivalent blackbody (EBB) temperatures as a function of zenith angle for LBL and CKD radiative transfer calculations based on 60 *g*-space intervals for tropical (TR), midlatitude summer (MLS), and midlatitude winter (MLW) profiles. Values for CKD given in terms of EBB temperature ($\Delta T_{ebb}$) and radiance ($\Delta I\uparrow$) differences and percentage difference (in parentheses). Positive differences represent overestimates by the CKD method.

| | | LBL | | CKD | |
|---|---|---|---|---|---|
| Profile | Zenith angle (deg) | $I\uparrow$ (W m$^{-2}$ sr$^{-1}$ $\mu$m$^{-1}$) | $T_{ebb}$ (K) | $\Delta I\uparrow$ (W m$^{-2}$ sr$^{-1}$ $\mu$m$^{-1}$, %) | $\Delta T_{ebb}$ (K, %) |
| TR | 16.20 | 8.631 | 294.31 | 0.012 (0.144) | 0.094 (0.032) |
| TR | 37.19 | 8.535 | 293.56 | 0.006 (0.067) | 0.047 (0.016) |
| TR | 58.30 | 8.291 | 291.62 | −0.012 (−0.140) | −0.096 (−0.033) |
| MLS | 16.20 | 8.139 | 290.40 | −0.015 (−0.181) | −0.121 (−0.042) |
| MLS | 37.19 | 8.080 | 289.93 | −0.023 (−0.282) | −0.187 (−0.064) |
| MLS | 58.30 | 7.922 | 288.64 | −0.043 (−0.543) | −0.353 (−0.122) |
| MLW | 16.20 | 5.914 | 270.79 | −0.028 (−0.475) | −0.272 (−0.100) |
| MLW | 37.19 | 5.900 | 270.66 | −0.034 (−0.573) | −0.331 (−0.122) |
| MLW | 58.30 | 5.861 | 270.28 | −0.048 (−0.819) | −0.469 (−0.174) |

TABLE 4. Same as Table 3 (60 $\Delta g$ intervals) except for clear-sky downwelling radiances and equivalent blackbody (EBB) temperatures at the surface.

| | | LBL | | CKD | |
|---|---|---|---|---|---|
| Profile | Zenith angle (deg) | $I\downarrow$ (W m$^{-2}$ sr$^{-1}$ $\mu$m$^{-1}$) | $T_{ebb}$ (K) | $\Delta I\downarrow$ (W m$^{-2}$ sr$^{-1}$ $\mu$m$^{-1}$, %) | $\Delta T_{ebb}$ (K, %) |
| TR | 163.80 | 4.689 | 258.10 | 0.029 (0.618) | 0.322 (0.125) |
| TR | 142.81 | 5.227 | 263.89 | 0.044 (0.839) | 0.458 (0.173) |
| TR | 121.70 | 6.443 | 275.80 | 0.084 (1.299) | 0.772 (0.280) |
| MLS | 163.80 | 3.026 | 237.07 | 0.020 (0.665) | 0.291 (0.123) |
| MLS | 142.81 | 3.439 | 242.85 | 0.027 (0.798) | 0.363 (0.149) |
| MLS | 121.70 | 4.470 | 255.62 | 0.051 (1.137) | 0.582 (0.228) |
| MLW | 163.80 | 0.496 | 177.22 | 0.034 (6.881) | 1.658 (0.935) |
| MLW | 142.81 | 0.577 | 181.05 | 0.038 (6.577) | 1.664 (0.919) |
| MLW | 121.70 | 0.801 | 189.95 | 0.047 (5.921) | 1.636 (0.861) |

than 0.4 K were obtained at all zenith angles. The poorest results are seen for the MLW profile, although the errors are acceptable ($<$0.5 K). The systematic errors for all profiles are comparable to the noise in the measurements. The increasing errors with decreasing total precipitable water are mainly the result of the increasing transmittance errors (refer to Table 2). For the most part, errors also tend to increase slightly with increasing zenith angle as the path becomes more opaque and the importance of atmospheric emission in this relatively transparent band increases. The exception, however, is the TR profile.

To further explore the effect of the transmittance errors on the TOA radiance, we present a simple error analysis example. Consider a purely absorbing/emitting, plane-parallel atmosphere overlying a blackbody surface. The monochromatic TOA radiance at nadir at wavelength $\lambda$ is expressed as

$$I_\lambda = B_\lambda(T_s)\tau_\lambda + \int_{p_s}^{0} B_\lambda[T(p)]\frac{\partial \tau_\lambda(p, 0)}{\partial p}\, dp, \quad (5)$$

where $B_\lambda$ is the Planck function, $T_s$ is the surface skin temperature, $\tau_\lambda$ is the total (or column) transmittance of the atmosphere, and $T(p)$ is the temperature profile as a function of pressure $p$. To simplify the error analysis the atmospheric emission term in (5) is parameterized as a function of $\tau_\lambda$. Using the three test atmospheres described previously, a suitable expression for this integral is $11[1 - \tau_\lambda]^{3/2}$ (W m$^{-2}$ sr$^{-1}$ $\mu$m$^{-1}$). Strictly speaking, the integral term is also dependent on the details of the water vapor profile; however, the parameterization was found to match the data well and is thus adequate for our purposes. The random error in the TOA radiance due to the uncertainty in the total atmospheric transmittance ($\sigma_\tau$) is given by

$$\sigma_I = \left|\sigma_\tau \frac{\partial I}{\partial \tau}\right| \approx |\sigma_\tau[B(T_s) - 16.5\sqrt{1 - \tau}]|, \quad (6)$$

where the wavelength dependence has been dropped for clarity. The uncertainty in the atmospheric transmittance can be estimated from the results of Table 2. While these results, being the difference from the LBL calculations (which are considered exact), are actually more a measure of the systematic errors, they will be used here to approximate the random errors. Uncertainties of 0.0112 and 0.0011 were therefore used for the MLW and TR profiles, respectively. The Planck function was evaluated using an OLS band-averaged wavelength of 11.358 $\mu$m. Inserting these values and the LBL transmittance values into (6) gives radiance errors of 0.0031 and 0.0115 W m$^{-2}$ sr$^{-1}$ $\mu$m$^{-1}$ for the TR and MLW profiles, respectively, thus confirming the dominant role of the transmittance errors in the TOA radiance errors.

Another way of evaluating the radiance errors is to compare instead the downwelling radiance at the surface, which is arguably more appropriate since the atmospheric component is isolated. Here, the errors are amplified somewhat as compared to the TOA radiances and EBB temperatures, with the largest error (0.77 K) for more moisture-laden atmospheres occurring for the TR profile at the smallest zenith angle (Table 4). Also, the MLS profile, rather than the TR profile, now has the smallest errors, though the differences between the profiles are small. For the MLW profile the errors climb to as high as 1.66 K. The errors generally increase with increasing zenith angle as well. The occurrence of larger errors for the downwelling radiances is mainly caused by $O_3$ absorption errors in the upper troposphere and lower stratosphere.

Given that the strongest absorption by $CO_2$ and $O_3$ occurs in spectral regions where the instrument response is relatively weak, it is possible to reduce the total number of calculations without greatly sacrificing modeling accuracy. If one neglects $\Delta g$ values less than or equal to 0.0025, then the number of RT calculations is reduced to 17. The TOA radiance and EBB temperature errors for this case are found to increase slightly for all profiles and zenith angles, as expected, but remain below 0.75 K (Table 5).

## 6. Summary

Application of an innovative and efficient CKD approach to the IR channel of the OLS yields sufficiently accurate estimates of the band-averaged atmospheric ab-

TABLE 5. Same as Table 3 except using only 17 $\Delta g$ intervals for correlated $k$-distribution method.

| | | LBL | | CKD | |
|---|---|---|---|---|---|
| Profile | Zenith angle (deg) | $I\uparrow$ (W m$^{-2}$ sr$^{-1}$ $\mu$m$^{-1}$) | $T_{ebb}$ (K) | $\Delta I\uparrow$ (W m$^{-2}$ sr$^{-1}$ $\mu$m$^{-1}$, %) | $\Delta T_{ebb}$ (K, %) |
| TR | 16.20 | 8.631 | 294.31 | −0.026 (−0.302) | −0.203 (−0.069) |
| TR | 37.19 | 8.535 | 293.56 | −0.031 (−0.368) | −0.244 (−0.083) |
| TR | 58.30 | 8.291 | 291.62 | −0.046 (−0.550) | −0.368 (−0.126) |
| MLS | 16.20 | 8.139 | 290.40 | −0.051 (−0.621) | −0.413 (−0.142) |
| MLS | 37.19 | 8.080 | 289.93 | −0.057 (−0.709) | −0.463 (−0.160) |
| MLS | 58.30 | 7.922 | 288.64 | −0.075 (−0.941) | −0.617 (−0.214) |
| MLW | 16.20 | 5.914 | 270.79 | −0.057 (−0.966) | −0.554 (−0.205) |
| MLW | 37.19 | 5.900 | 270.66 | −0.062 (−1.050) | −0.604 (−0.223) |
| MLW | 58.30 | 5.861 | 270.28 | −0.074 (−1.266) | −0.724 (−0.268) |

sorption for use in detailed remote sensing studies. Several aspects of this approach set it apart from conventional CKD methods. Foremost, it saves wavenumber information at the $g$-space level. This enables overlapping absorption to be isolated and treated in a more efficient manner. It also allows one to determine the source functions and include details of the instrument response function at the $g$-space level, which is a major advantage over previous CKD approaches. In addition, the present CKD method is implemented in the context of an error minimization philosophy, which is a new approach to the problem.

In terms of the impact on the forward calculation of TOA upwelling EBB temperatures, the systematic errors attributed to the CKD method using 60 $g$-space intervals tend to increase with decreasing total water vapor amounts and column absorption/emission, and increase with increasing zenith angle. For all profiles these errors are no larger than 0.5 K. For downwelling EBB temperatures at the surface the errors become somewhat larger. For the TR and MLS profiles the largest error is 0.77 K. The maximum error of 1.66 K occurs for the MLW profile. Radiative transfer calculations using as few as 17 $g$-space intervals can provide reasonable errors in the TOA EBB temperatures ($<$0.75 K) for a broad range of atmospheres and zenith angles. However, the use of at least 60 $g$-space intervals is recommended for drier atmospheres.

*Acknowledgments.* Support for this work was provided by NASA Grant NAG5-3449, the National Space Development Agency of Japan (NASDA) Grant A-0011, and DOD Center for Geosciences Grant DAAL01-98-2-0078 MOD 01. C. Drummond was supported by NASA Earth System Science Fellowship Grant NGT5-50007. The OLS data were obtained from the National Geophysical Data Center (NGDC). Special thanks go to Robert Carrell at Northrop Grumman for supplying the OLS spectral response curve and other pertinent information. We also thank Sundar Christopher at the University of Alabama in Huntsville for providing the AVHRR spectral response curves and Andrew Jones for his remarks on the manuscript.

## REFERENCES

Ambartzumian, V., 1936: The effect of the absorption lines on the radiative equilibrium of the outer layers of the stars. *Pupl. Obs. Astron. Univ. Leningrad,* **6,** 7–18.

Brandli, H. W., D. L. Reinke, and L. E. Irvin, 1977: Sea surface emission temperatures from Defense Meteorological Satellite. *J. Phys. Oceanogr.,* **7,** 302–304.

Buettner, K. J. K., and C. D. Kern, 1965: The determination of infrared emissivities of terrestrial surfaces. *J. Geophys. Res.,* **70,** 1329–1337.

Cahoon, 1992: Seasonal distribution of African savannah fires. *Nature,* **359,** 812–815.

Clough, S. A., F. X. Kneizys, and R. W. Davies, 1989: Line shape and the water vapor continuum. *Atmos. Res.,* **23,** 229–241.

Cogan, J. L., 1976: Interpretation of 8–13 $\mu$m measurements of sea-surface temperature. *Quart. J. Roy. Meteor. Soc.,* **102,** 771–774.

Drummond, C. J., and G. L. Stephens, 1998: A novel $k$-distribution parameters development system and its application to MAS/SUCCESS channels. Atmospheric Science Paper No. 645, Colorado State University, 84 pp. [Available from Department of Atmospheric Science, Colorado State University, Fort Collins, CO 80523.]

Fett, R. W., 1993: The Kamishak Gap wind as depicted in DMSP OLS and SSM/I data. *Int. J. Remote Sens.,* **14,** 403–423.

Formichev, V. I., and G. M. Shved, 1995: Parameterization of the radiative flux divergence in the 9.6 $\mu$m $O_3$ band. *J. Atmos. Terr. Phys.,* **47,** 1037–1049.

Fu, Q., and K. N. Liou, 1992: On the correlated $k$-distribution method for radiative transfer in nonhomogeneous atmospheres. *J. Atmos. Sci.,* **49,** 2139–2156.

Goodman, S. J., and H. J. Christian, 1993: Global observations of lightning. *Atlas of Satellite Observations Related to Global Change.* R. J. Gurney, J. L. Foster, and C. L. Parkinson, Eds., Cambridge University Press, 191–219.

Goody, R. M., and Y. L. Yung, 1989: *Atmospheric Radiation Theoretical Basis.* Oxford University Press, 519 pp.

Isaacs, R. G., and J. C. Barnes, 1987: Intercomparison of cloud imagery from the DMSP OLS, NOAA AVHRR, GOES VISSR, and Landsat MSS. *J. Atmos. Oceanic Technol.,* **4,** 647–667.

Jones, A. S., and T. H. Vonder Haar, 1997: Retrieval of microwave surface emittance over land using coincident microwave and infrared satellite measurements. *J. Geophys. Res.,* **102,** 13 609–13 626.

Kratz, D. P., 1995: The correlated $k$-distribution technique as applied to the AVHRR channels. *J. Quant. Spectrosc. Radiat. Transfer,* **53,** 501–517.

Lacis, A. A., and J. E. Hansen, 1974: Parameterization for the absorption of solar radiation in the earth's atmosphere. *J. Atmos. Sci.,* **31,** 118–133.

——, and V. Oinas, 1991: A description of the correlated $k$-distribution method for modeling nongray gaseous absorption, ther-

mal emission and multiple scattering in vertically inhomogeneous atmospheres. *J. Geophys. Res.*, **96**, 9027–9063.

May, D. A., 1993: Sea surface temperature estimation from the DMSP operational linescan system using a SSM/I-derived water vapor correction. *Geophys. Res. Lett.*, **20,** 583–586.

McClatchey, R. A., R. W. Fenn, J. E. Selby, F. E. Voltz, and J. S. Garing, 1972: Optical properties of the atmosphere. 3d ed. AFCRL Environmental Research Paper 411, 108 pp. [Available from Air Force Cambridge Research Laboratories, Hanscom AFB, Bedford, MA 01731.]

Roberts, R. E., J. E. A. Selby, and L. M. Biberman, 1976: Infrared continuum absorption by atmospheric water vapor in the 8–12 $\mu$m window. *Appl. Opt.*, **15,** 2085–2090.

Rothman, L. S., and Coauthors, 1992: The HITRAN molecular database editions of 1991 and 1992. *J. Quant. Spectosc. Radiat. Transfer*, **48,** 469–507.

Spangler, M. J., 1974: The DMSP primary data sensor. *Proc. Sixth Conf. on Aerospace and Aeronautical Meteorology*, El Paso, TX, Amer. Meteor. Soc., 150–157.